International Journal of Minerals, Metallurgy and Materials
Volume 26, Number 1, January 2019, Page 124
https://doi.org/10.1007/s12613-019-1716-x

Azo dye degradation behavior of AlFeMnTiM (M = Cr, Co, Ni) high-entropy alloys

Shi-kai Wu, Ye Pan, Ning Wang, Tao Lu, and Wei-ji Dai

School of Materials Science and Engineering, Southeast University, Jiangsu Key Laboratory for Advanced Metallic Materials, Nanjin 211189, China
(Received: 10 March 2018; revised: 30 June 2018; accepted: 29 July 2018)

Abstract: Because of the potential carcinogenic effects and difficult degradation of azo dyes, their degradation has been a longstanding problem. The degradation of azo dye Direct Blue 6 (DB6) using ball-milled (BM) high-entropy alloy (HEA) powders was characterized in this work. Newly designed AlFeMnTiM (M = Cr, Co, Ni) HEAs synthesized by mechanical alloying (MA) showed excellent performance in the degradation of azo dye DB6. The degradation efficiency of AlFeMnTiCr is approximately 19 times greater than that of the widely used commercial Fe–Si–B amorphous alloy ribbons and more than 100 times greater than that of the widely used commercial zero-valent iron (ZVI) powders. The galvanic-cell effect and the unique crystal structure are responsible for the good degradation performance of the BM HEAs. This study indicates that BM HEAs are attractive, valuable, and promising environmental catalysts for wastewater contaminated by azo dyes.

Keywords: high entropy alloy; mechanical alloying; AlFeMnTiM; degradation performance; azo dye

1. Introduction

Azo dyes are characterized by one or more –N=N– groups, and they account for 60%–70% of synthetic dyes in the dye market. Azo dyes are used in commercial applications such as dyeing of various fibers, leather, paper, candles, ink, plastics, and food, and their use increases from year to year [1–4]. The wastewater polluted by azo dyes has always been a concern for researchers because of their potential carcinogenic effect on humans [5–7]. Various methods to remove azo dyes from aqueous solution have been used, including physical adsorption, oxidation processes, biological methods, and degradation by metallic glasses or zero-valent metals, etc. [1,8–16]. However, all of these methods have disadvantages; for instance, physical adsorption may be ineffective, oxidation processes such as photocatalysis are expensive, and biodegradation is often kinetically slow. Metallic glasses and zero-valent metals are attracting increasing interest from researchers because of their fine capacity to deal with azo dye wastewater; however, they also suffer numerous disadvantages [3,16–25]. For example, metallic glasses exhibit excellent capability to degrade azo dyes, as reported by many researchers, but the conditions required for the synthesis of metallic glasses are very strict. These conditions include, for example, the use of high-purity raw materials, high-vacuum equipment, high cooling speeds, and strict component design [16,26–28]. Zero-valent iron (ZVI) is a typical environmentally friendly zero-valent metal. Because of its strong reducibility, it exhibits a strong ability to reduce and degrade azo dyes; however, the stability of small ZVI particles is poor, and they easily recombine and oxidize during the reaction process [7,9,29–30]. Moreover, developing a material that is inexpensive, easily prepared, and highly efficient at degrading azo dyes is a high priority.

As a new type of material, high-entropy alloys (HEAs) have received extensive attention in the materials science community in recent decades; however, previous research on HEAs has mainly focused on their mechanical properties [31–36]. Given the good catalytic performance of metallic glasses and ZVI powders, HEAs are expected to exhibit remarkable functional capacity in the degradation of dye

Corresponding author: Ye Pan E-mail: panye@seu.edu.cn

effluents. Lv *et al*. [5] have reported that an AlCoCrTiZn HEA synthesized by mechanical alloying (MA) exhibits a substantial capacity in the degradation of azo dye Direct Blue 6 (DB6), as high as that of the MgZn-based glass, which is the best-performing azo-dye degradation catalyst among the metallic glasses thus far [28]. Although HEAs exhibit excellent capacity to degrade azo dyes, their application as azo-dye degradation catalysts has attracted little attention and the literature contains few reports on the degradation of azo dyes by HEAs. The purpose of this work is to develop novel HEA systems for the degradation of azo dyes. Moreover, the degradation mechanisms, decomposition kinetics, and degradation efficiency warrant further exploration.

The degradation capacity of three new HEAs—AlFeMnTiCr (Sample 1, denoted as S_{Cr}), AlFeMnTiCo (Sample 2, denoted as S_{Co}), and AlFeMnTiNi (Sample 3, denoted as S_{Ni}) in degrading an aqueous solution of azo dye DB6 is reported in the present work. Our findings may extend the applications of HEAs as functional materials.

2. Experimental

Al, Co, Cr, Fe, Mn, Ni, and Ti elemental powders with high purity (>99.9wt%) and particle sizes smaller than 45 μm were used as raw materials to synthesize equiatomic S_{Cr}, S_{Co}, and S_{Ni} HEAs by MA. Compared with rare-earth elements or noble metals, the elements used in this work are all relatively common, inexpensive, and environmentally friendly. The ball-milling process was carried out in a high-energy planetary ball mill at a speed of 400 r/min and a ball-to-powder ratio of 20:1. Zirconia jars and balls were used as the milling media, and stearic acid was used as the process control agent (PCA) to prevent excessive cold welding. After 50 h of milling, the BM HEA powders were removed from the zirconia jars for further characterization. To avoid over heating during the ball-milling process, the ball mill was set to rotate for 1 h, halt for 10 min, and then repeat the cycle until the set time point was reached. High-purity Ar was charged into each ball jar before ball milling to prevent oxidation of the raw powders.

The Fe–Si–B amorphous alloys with a nominal composition of $Fe_{78}Si_{13}B_9$ (atomic ratio) were purchased from Antai Co. (Beijing, China). The 300-mesh ZVI powders (purity > 99.9%) were provided by Cuiboling Co. (Beijing, China). DB6 ($C_{32}H_{20}N_6S_4O_{14}Na_4$) was purchased from Hailan Chemical Pigment Co. (Tianjin, China). The beaker for the degradation of azo dye DB6 was placed in a constant-temperature water bath, and the mechanical stirring was carried out at a fixed speed in the beaker during the reaction. For each degradation test, 0.1 g of HEA powder was added to 100 mL of an azo dye DB6 solution with a dye concentration of 200 mg/L for reaction; distilled water was used as the solvent throughout the experiments. At preset reaction-time intervals, approximately 3 mL of solution was removed from the dye solution and centrifuged to remove the HEA powder; the centrifuged solution was then scanned in an ultraviolet–visible (UV–Vis) spectrophotometer over the wavelength range from 400 to 800 nm. The degradation of DB6 was conducted at an HEA concentration of 1 g/L and a DB6 azo dye concentration of 200 mg/L, without the addition of any other reagents.

The crystal structure of the samples was studied by X-ray diffraction (XRD, D8 Advance, Cu K_α) and transmission electron microscopy (TEM, Tecnai FEI F20). The morphology and size distribution of the milled powders were studied by scanning electron microscopy (SEM, JSM-7100F), and the compositions were examined by energy-dispersive X-ray spectroscopy (EDS) using a spectrometer equipped on the scanning electron microscope. The statistical distribution of the particle size was recorded with a laser particle analyzer (FJUL1076), and the particles' surface area analysis was performed by the Brunauer–Emmett–Teller (BET) technique (3H-2000BET-A) using the nitrogen adsorption method. The concentrations of the metal ions remaining in the degraded dye solutions were detected by inductive coupled plasma atomic emission spectroscopy (ICP-AES, PerkinElmer ICP8000), and a digital pH meter (FE20, Mettler Toledo) was used to measure the pH values of DB6 solutions. The UV–Vis absorption spectra were recorded using a UV–Vis spectrometer (TU-1810). A laboratory electric mechanical agitator (JB90-D) was rotated at a certain speed in the present work to distribute the HEA powders uniformly in the dye solution.

3. Results and discussion

3.1. Characterization of S_{Cr}, S_{Co} and S_{Ni} HEAs

The XRD patterns of the S_{Cr}, S_{Co}, and S_{Ni} samples are presented in Fig. 1, demonstrating the presence of two simple solid–solution phases (FCC phase and BCC phase) without other intermetallic compounds. This phenomenon indicates that the three HEAs are completely alloyed during the MA process. The peaks of FCC (111) and BCC (110) at $2\theta = 43.2°$ and 44.6°, respectively, appear in the patterns of all three of the HEAs; however, the BCC (200) and (220) reflections at $2\theta = 65.0°$ and 82.3°, respectively, appear only in the patterns of S_{Cr} and S_{Co}.

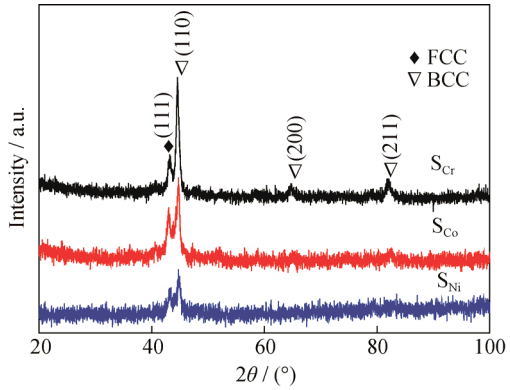

Fig. 1. XRD patterns of the AlFeMnTiM (M = Cr, Co, Ni) HEAs.

The good catalytic properties of many nanostructured materials are obviously dependent on their morphologies, crystallite size, and distribution. As depicted in Fig. 2, the particle sizes of the S_{Cr}, S_{Co}, and S_{Ni} samples exhibit a relatively uniform distribution and the surface of the powders is rough, with many corrugations and micropores. These results indicate that the three HEA powders exhibit high specific surface areas with abundant active sites. In the process of degrading azo dye DB6, the HEA powders are uniformly distributed in the dye solution through mechanical mixing by the electric mechanical agitator, which promotes the reaction between the powders and the dye solution. The structure of S_{Cr} was further characterized by TEM bright-field imaging (Fig. 3(a)); its corresponding selected-area electron diffraction (SAED) pattern is shown in Fig. 3(b). The crystalline nature of S_{Cr} was also clearly confirmed by high-resolution TEM (HRTEM) (Fig. 3(c)). The lattice fringes (highlighted with white lines in Fig. 3(c)) correspond to 02097 nm; thus, according to the data in the PDF card, its corresponding crystal face is the (111) plane of the FCC phase.

The EDS analysis results for the S_{Cr} sample are presented in Fig. 4. These results reveal that the as-produced BM particles are composed of Al, Cr, Fe, Mn, and Ti, with no substantial traces of other elements, and that the ratio of these

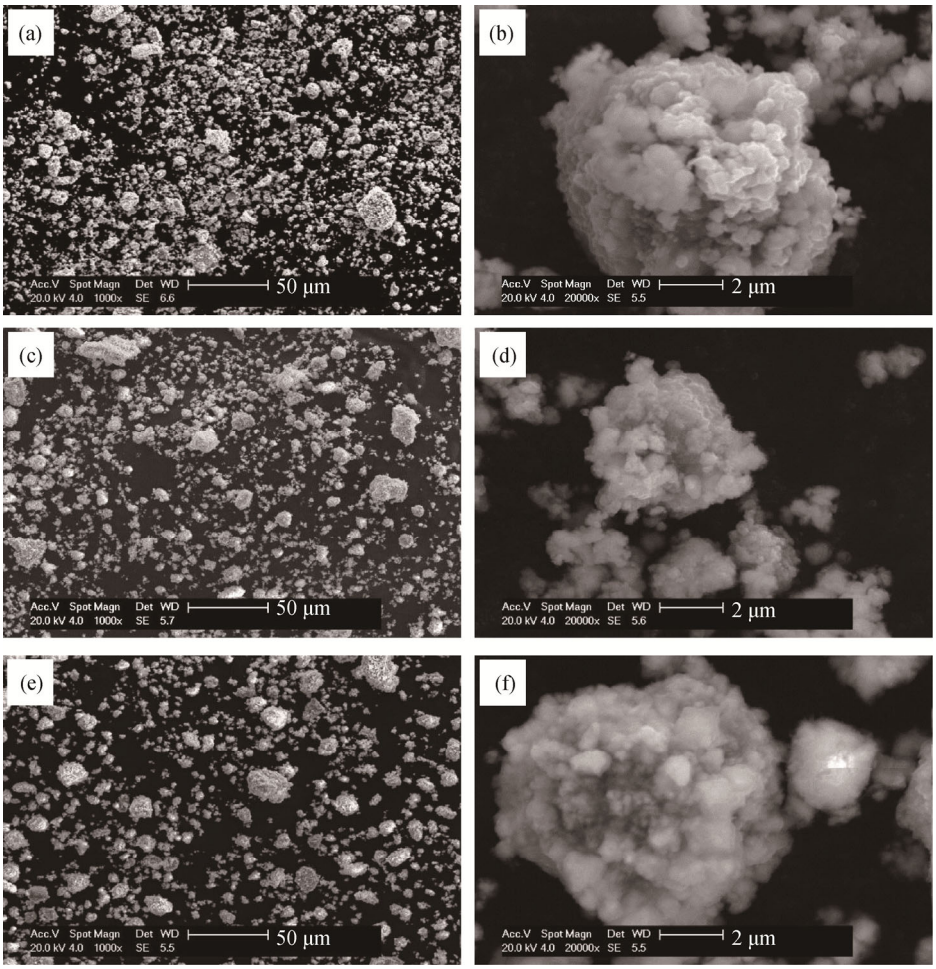

Fig. 2. SEM images of the AlFeMnTiM (M = Cr, Co, Ni) HEAs: (a) and (b) S_{Cr}; (c) and (d) S_{Co}; (e) and (f) S_{Ni}.

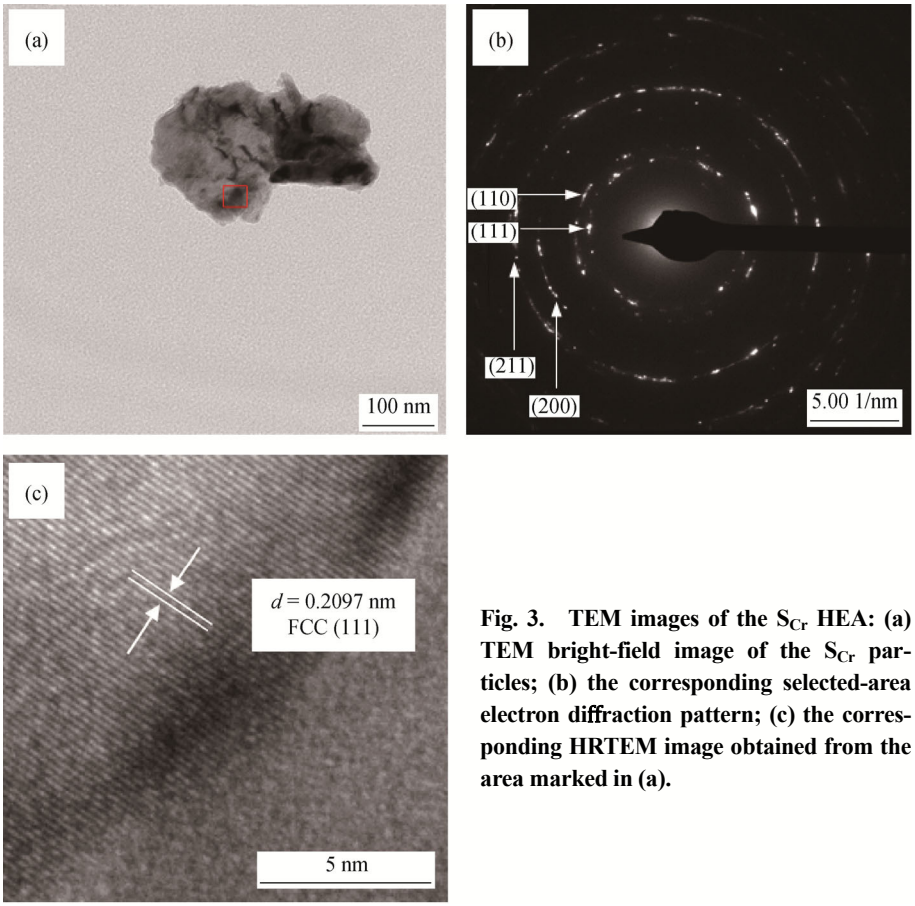

Fig. 3. TEM images of the S_{Cr} HEA: (a) TEM bright-field image of the S_{Cr} particles; (b) the corresponding selected-area electron diffraction pattern; (c) the corresponding HRTEM image obtained from the area marked in (a).

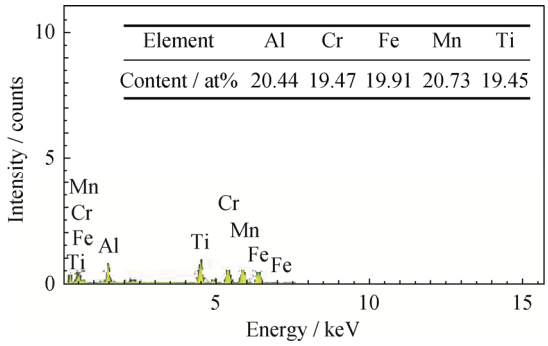

Fig. 4. EDS analysis results showing the actual composition of S_{Cr}.

elements in each sample is approximately 1:1:1:1:1, in good agreement with the nominal composition of S_{Cr}. The average particle diameters of S_{Cr}, S_{Co}, and S_{Ni} are 8.2, 8.5, and 7.8 μm, respectively, as measured by the laser particle analyzer. The size distributions of most of the three HEA powders range from 1 to 20 μm, and the size of the smaller particles is close to the nanoscale. To understand the high reaction efficiency of the HEA powders, we measured their specific surface areas, which were 6.08, 6.48, and 6.31 m^2/g for S_{Cr}, S_{Co}, and S_{Ni}, respectively. Their surface areas are clearly very similar.

3.2. Degradation of azo dye DB6 by the HEAs

DB6 is an industrial azo dye used to simulate actual wastewater applications [5]. The degradation of DB6 by HEAs in the present study is characterized on the basis of UV–Vis absorption spectra. As an example, the UV–Vis absorption spectra corresponding to the degradation of DB6 by S_{Cr} are presented in Fig. 5. The decrease in the intensity of the absorption peak suggests degradation of the DB6 solution.The degradation of the dye occurs immediately upon the addition of the S_{Cr} powder into the dye solution, and the degradation process is completed in approximately 11 min. At t = 0 min, the curve represents the absorption spectra of the DB6 solution before degradation. The –N=N– bonds in the DB6 molecules are the chromophoric groups responsible for their color, and the absorption peak occurred at 574 nm [5,21]. As illustrated, the absorption peak decreases in intensity with the addition of the HEA powders, indicating cleavage of the –N=N– bonds [37]. The degradation products are likely aniline, benzene homologues, and some small organic molecules without chromophore groups, which are low-toxicity, easily mineralized compounds with strong biodegradability and no prominent effect on the color of the dye solution [38–39].

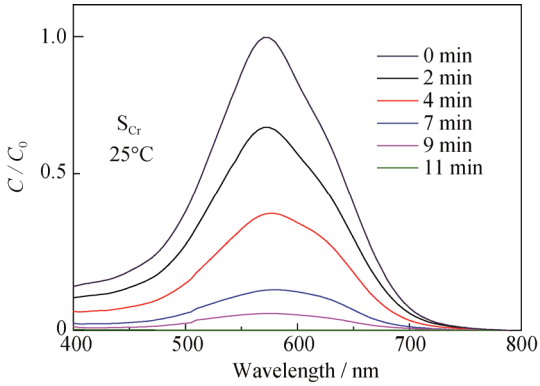

Fig. 5. UV–vis spectra and normalized concentration of DB6 during decomposition by S_{Cr} at 25°C and an initial pH value of 7 (C is the concentration of the DB6 solution which is taken from the centrifugal tube, and C_0 is the primary concentration of the DB6 solution).

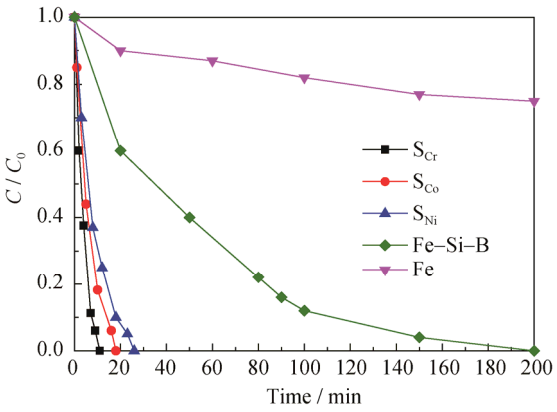

Fig. 6. Degradation curves of the 200 mg/L DB6 solution degraded by 1 g/L S_{Cr}, 1 g/L S_{Co}, 1 g/L S_{Ni}, 1 g/L Fe–Si–B amorphous alloy ribbons, and 1 g/L ZVI powders, respectively, during the decomposition process at 25°C and an initial pH value of 7.

Fig. 6 presents the degradation efficiency of 200 mg/L DB6 solution degraded by 1 g/L S_{Cr}, S_{Co}, S_{Ni}, Fe–Si–B amorphous alloy ribbons, and ZVI at 25°C and an initial pH value of 7. Because of their excellent capacity to degrade azo dye DB6 solution, the Fe–Si–B amorphous alloy and ZVI have been extensively investigated by many researchers; they were therefore selected as the reference materials in the present work. Nonlinear curve fitting reveals that the degradation process of DB6 with the five aforementioned materials exhibits kinetics consistent with a pseudo-frst-order kinetic model [5,38]:

$$I = I_1 + I_2 \exp(-t/t_0)$$

where I is the normalized intensity of concentration, I_1 and I_2 are ftting constants, t is the reaction time, and t_0 is the time when the intensity decreases to e^{-1} of the initial condition.

The S_{Cr}, S_{Co}, and S_{Ni} demonstrate excellent performance in the degradation of DB6, much better than that of commercial Fe–Si–B amorphous alloys and ZVI. The whole degradation time of DB6 by S_{Cr}, S_{Co}, S_{Ni}, and Fe–Si–B are 11, 22, 30, and 200 min, respectively. The ZVI powder degraded less than 25% of the DB6 solution. The degradation efficiency of S_{Cr} is approximately 19 times greater than that of the widely used commercial Fe–Si–B amorphous alloy ribbons and more than 100 times greater than that of the widely used commercial ZVI powders. According to the activity series of metals [5], the activity rank of the constituent elements in the three HEAs is Al > Ti > Mn > Cr > Fe > Co > Ni. The degradation efficiency of the three HEA powders decreases in the order of $S_{Cr} > S_{Co} > S_{Ni}$, consistent with the activity rank of the constituent elements Cr, Co, and Ni. This result also indicates that the activity of the constituent elements strongly influences the degradation capacity of HEAs.

On the basis of the kinetic rate constants obtained at different temperatures, the activation energy (ΔE, kJ·mol^{-1}) of the degradation process of DB6 by the HEAs was obtained according to the following equation [5,39]:

$$t_0 = \tau_0 \exp[\Delta E/(RT)]$$

where τ_0 is a time pre-factor and R is the gas constant. The normalized concentration as a function of treatment time of the degradation of DB6 by S_{Cr} at different temperatures ranging from 25 to 55 °C is depicted in Fig. 7(a). A plot of $\ln t_0$ vs. $1000/(RT)$ for estimating the activation energy of degradation of DB6 by S_{Cr} is shown in Fig. 7(b) (initial pH = 7, 1 g/L S_{Cr}). For ordinary thermal reactions, the activation energy is typically between 60 and 250 kJ·mol^{-1} [40]. However, the activation energy of S_{Cr} is just 47.4 kJ·mol^{-1} for degrading azo dye DB6. Our results imply that the degradation of DB6 by HEAs requires a relatively low energy, which may also explain why the HEAs show excellent performance in degrading azo dyes.

Surface micrographs of S_{Cr}, S_{Co}, and S_{Ni} after degradation are provided in Fig. 8; they demonstrate that nanobristles uniformly and loosely distribute on the surfaces of the three HEA powders. The surface micrographs of the three degraded powders also indicate that the three BM HEA powders exhibit high activity. The nanowhiskers are dense, indicating homogenous corrosion on the surface. As presented in Fig. 8(d), the EDS analysis results indicate that these nanobristles are mainly composed of Al, Fe, and O. The pH values of the DB6 solution after being completely degraded by the S_{Cr}, S_{Co} and S_{Ni} powders are 9.0, 8.5, and 8.8, respectively, which means that the solutions are all alkaline after degradation. As evident from Fig. 9, the composition of S_{Cr} changes somewhat after degradation of DB6. In addition to

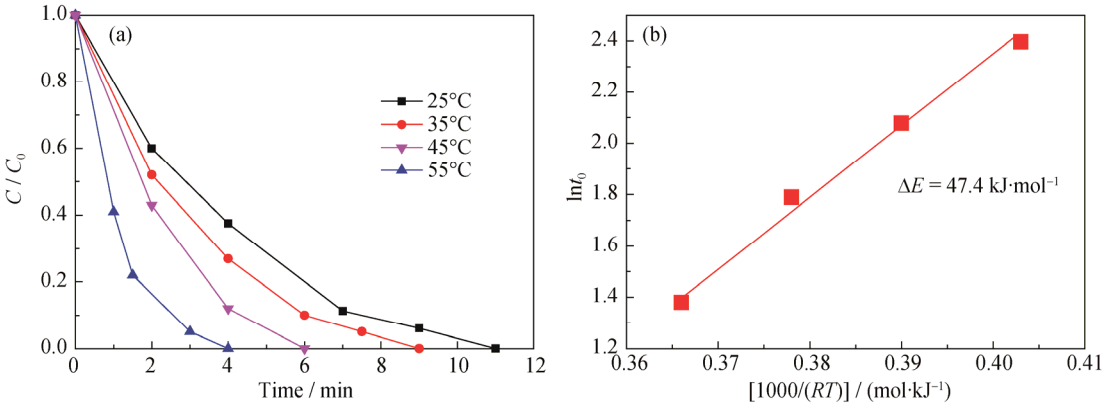

Fig. 7. Normalized concentration as a function of treatment time in the degradation of DB6 by S_{Cr} at temperatures ranging from 25 to 55 °C (a) and plot of $\ln t_0$ vs. 1000/(RT) for estimating the activation energy of degradation of DB6 by S_{Cr} (b) (initial pH = 7, 1 g/L S_{Cr}).

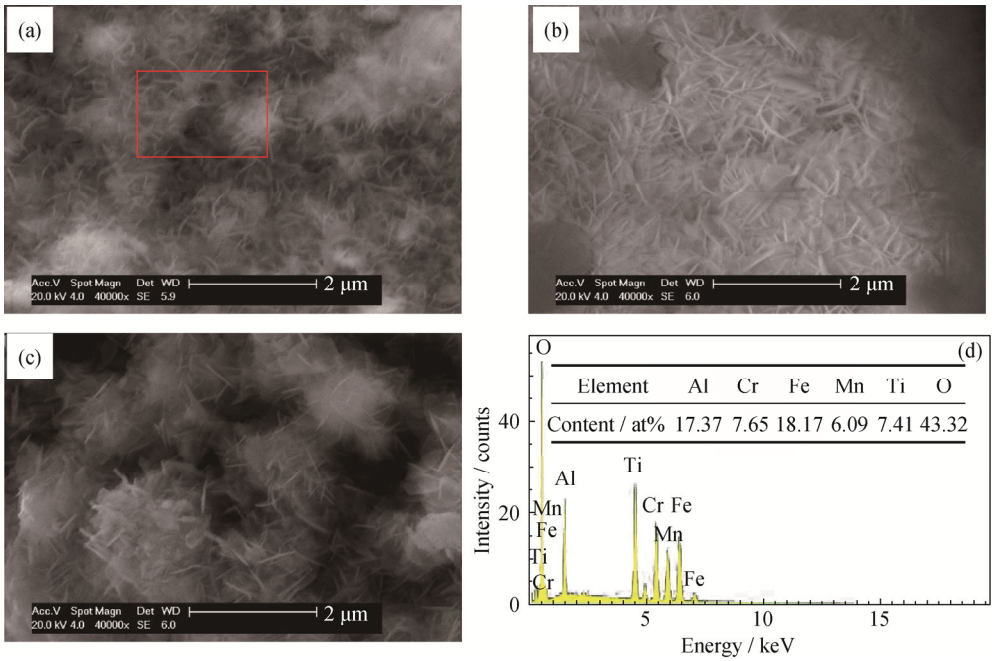

Fig. 8. SEM images and EDS spectrum of the AlFeMnTiM (M = Cr, Co, Ni) HEAs after degradation: (a) SEM image of S_{Cr}; (b) SEM image of S_{Co}; (c) SEM image of S_{Ni}; (d) EDS spectrum of S_{Cr} corresponding to the region in the red frame in (a).

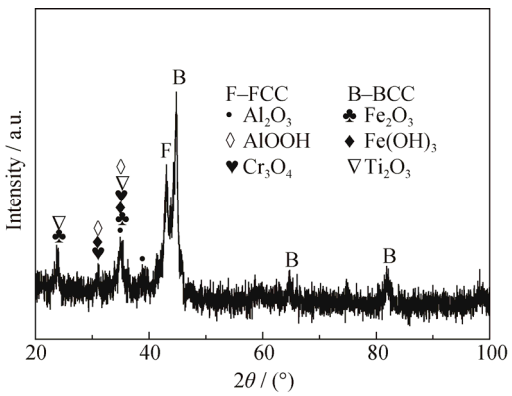

Fig. 9. XRD curves of the S_{Cr} HEA after degradation of DB6.

the FCC and BCC phases, the surface of S_{Cr} contains Al_2O_3, Fe_2O_3, Cr_3O_4, Ti_2O_3, AlOOH, and $Fe(OH)_3$. These phases form because, in the process of azo dye degradation, metals reduce the azo dyes and are oxidized to metal ions, which combine with oxygen in water to generate oxides such as Al_2O_3, Fe_2O_3, Cr_3O_4, and Ti_2O_3. Metal ions also combine with hydroxyl ions in water to produce hydroxides such as AlOOH and $Fe(OH)_3$. In addition, Table 1 shows that the concentration of each ion remaining in the solution is very low, approaching the lower limit of detection of the instrument. The ICP-AES results indicate that the three HEAs do not cause secondary pollution during the degradation process.

Table 1. Ion concentration in the degraded solution 10^{-6}

Ion	S_{Cr}	S_{Co}	S_{Ni}
Al	0.004	0.0672	0.004
Fe	0.013	0.013	0.013
Mn	0.7495	0.001	0.1329
Ti	0.001	0.006	0.006
Cr	0.012	—	—
Co	—	0.008	—
Ni	—	—	0.012

3.3. Degradation reaction mechanism analysis

The –N=N– bonds are known to be the most active bonds in azo dye molecules, and the cleavage of –N=N– bonds leads to the degradation of azo dyes [41]. During the ball-milling process, severe plastic deformation is induced, resulting in stress, strain, and lattice distortion and simultaneously introducing numerous defects into the HEAs particles; consequently, the surface and lattice distortion energy of the powders are greatly increased. The BM HEA powders are in a thermodynamically metastable state with excellent degradation capability; this state is unachievable in conventional alloys. Thus, the excellent degradation performance of azo dye DB6 by S_{Cr}, S_{Co}, and S_{Ni} is attributed to the following three main factors.

First, compared with the surface of pure single metals, the surface of the BM HEAs are electrochemically inhomogeneous because of the HEAs' special alloy components and severe lattice distortion; this inhomogeneity results in the formation of a large number of nano-galvanic cells among the elements, which is the dominant factor responsible for the good degradation performance of S_{Cr}, S_{Co} and S_{Ni} powders. Two different elements and a dye solution make up a nano-galvanic cell, and a large amount of nano-galvanic cells occupy the surface of HEAs. The active metals act as cathodes that lose electrons, the inactive positive metals act as anodes that receive electrons and catalyze azo dye molecules, generating hydrogen ions and electrons; the azo bonds are broken after the dye molecules combine with the hydrogen ions and electrons. The reaction process is shown in the following formulas:

$$M \rightarrow M^{n+} + ne^- \quad (1)$$

$$H_2O \rightarrow H^+ + OH^- \quad (2)$$

$$R{-}N{=}N{-}R_1 \xrightarrow{+\,4H^+ + 4e^-} R{-}NH_2 + R_1{-}NH_2 \quad (3)$$

The effect of the galvanic cells enables the BM HEAs to continuously release a large number of electrons; this reaction is much faster and releases far more electrons than the corresponding reaction of ordinary single zero-valent metals.

Second, the combination of a unique crystal structure with severe lattice distortion, residual stress, and stored plastic deformation energy is responsible for the excellent degradation capacity of BM HEAs toward azo dyes. The unique solid-solution structure of HEAs is in a nonequilibrium state in which atoms possess high potential energy; in addition, the surface of the HEAs has many more active sites than conventional alloys.

Third, the reduction behavior of nascent hydrogen ([H]) likely plays a role. A large number of electrons are released by S_{Cr}, S_{Co}, and S_{Ni}, and hydrogen ions in water combine with electrons to form nascent hydrogen, [H]. The [H] is a rapid reduction agent that has been found to reduce various organic species. The [H] exhibits high reactivity, induces the cleavage of azo bonds, and destroys the chromophore groups.

4. Conclusions

(1) S_{Cr}, S_{Co}, and S_{Ni} were successfully fabricated by the MA technique. Their efficiency and reaction kinetics in degrading organic chemicals were systematically investigated through evaluation of their degradation capability for azo dye DB6. The S_{Cr}, S_{Co}, and S_{Ni} exhibited excellent degradation efficiency in the degradation of azo dye DB6.

(2) In particular, S_{Cr} exhibited superior degradation efficiency and good catalytic activity; its degradation performance toward DB6 is much better than that of the common commercial Fe–Si–B amorphous alloys and ZVI powders, and its thermal activation energy barrier (ΔE = 47.4 kJ.mol^{-1}) is low.

(3) The perfect performance of S_{Cr}, S_{Co}, and S_{Ni} in the degradation of azo dye DB6 is attributed to the galvanic-cell effect, unique crystal structures, severe lattice distortion, special alloy compositions, and reduction reactions. The BM HEAs are promising and efficient materials for textile water discoloration treatment.

Acknowledgements

This work was financially supported by the National Natural Science Foundation of China (No. 51671056), Jiangsu Key Laboratory for Advanced Metallic Materials (No. BM2007204).

References

[1] H.N. Liu, G.T. Li, J.H. Qu, and H.J. Liu, Degradation of azo dye Acid Orange 7 in water by Fe^0/granular activated carbon

system in the presence of ultrasound, *J. Hazard. Mater.*, 144(2007), No. 1-2, p. 180.

[2] B. Chen, X.K. Wang, C. Wang, W.Q. Jiang, and S.P. Li, Degradation of azo dye direct sky blue 5B by sonication combined with zero-valent iron, *Ultrason. Sonochem.*, 18(2011), No. 5, p. 1091.

[3] J.H. Ramirez, F.J. Maldonado-Hódar, A.F. Pérez-Cadenas, C. Moreno-Castilla, C.A. Costa, and L.M. Madeira, Azo-dye Orange II degradation by heterogeneous Fenton-like reaction using carbon–Fe, *Appl. Catal. B*, 75(2007), No. 3-4, p. 312.

[4] Y.C. Dong, L.C. He, and M. Yang, Solar degradation of two azo dyes by photocatalysis using Fe(III)-oxalate complexes/H_2O_2 under different weather conditions, *Dyes Pigm.*, 77(2008), No. 2, p. 343.

[5] Z.Y. Lv, X.J. Liu, B. Jia, H. Wang, Y. Wu, and Z.P. Lu, Development of a novel high-entropy alloy with eminent efficiency of degrading azo dye solutions, *Sci. Rep*., 6(2016), No. 4, p. 34213.

[6] Y.N. Liu, H. Tian, and A.H. Si, Gliding arc discharge for decolorization and biodegradability of azo dyes and printing and dyeing wastewater, *Plasma Chem. Plasma Process.*, 32(2012), No. 3, p. 597.

[7] H.L. Lv, H.Y. Zhao, T.C. Cao, L. Qian, Y.B. Wang, and G.H. Zhao, Efficient degradation of high concentration azo-dye wastewater by heterogeneous Fenton process with iron-based metal-organic framework, *J. Mol. Catal. A: Chem.*, 400(2015), No. 3, p. 81.

[8] R. Patel and S. Suresh, Decolourization of azo dyes using magnesium-palladium system, *J. Hazard. Mater.*, 137(2006), No. 3, p. 1729.

[9] S.H. Chang, K.S. Wang, S.J. Chao, T.H. Peng, and L.C. Huang, Degradation of azo and anthraquinone dyes by a low-cost Fe^0/air process, *J. Hazard. Mater.*, 166(2009), No. 2-3, p. 1127.

[10] J.M. Kwon, Y.H. Kim, B.K. Song, S.H. Yeom, B.S. Kim, and J.B. Im, Novel immobilization of titanium dioxide (TiO_2) on the fluidizing carrier and its application to the degradation of azo-dye, *J. Hazard. Mater.*, 134(2006), No. 1-3, p. 230.

[11] E.S. Aazam and R.M. Mohamed, Environmental remediation of direct blue dye solutions by photocatalytic oxidation with cuprous oxide, *J. Alloys Compd.*, 577(2013), No. 45, p. 550.

[12] P. Singla, M. Sharma, O.P. Pandey, and K. Singh, Photocatalytic degradation of azo dyes using Zn-doped and undoped TiO_2 nanoparticles, *Appl. Phys. A*, 116(2014), No. 1, p. 371.

[13] N. Divya, A. Bansal, and A.K. Jana, Photocatalytic degradation of azo dye Orange II in aqueous solutions using copper-impregnated titania, *Int. J. Environ. Sci. Technol.*, 10(2013), No. 6, p. 1265.

[14] A. Pandey, P. Singh, and L. Iyengar, Bacterial decolorization and degradation of azo dyes, *Int. Biodeterior. Biodegrad.*, 59(2007), No. 2, p. 73.

[15] A.D. Bokare, R.C. Chikate, C.V. Rode, and K.M. Paknikar, Effect of surface chemistry of Fe–Ni nanoparticles on mechanistic pathways of azo dye degradation, *Environ. Sci. Technol.*, 41(2007), No. 21, p. 7437.

[16] X. Liu, L. Huang, D.S. Zhang, T.T. Yan, J.P. Zhang, and L.Y. Shi, Light driven fabrication of highly dispersed Mn–Co/RGO and the synergistic effect in catalytic degradation of methylene blue, *Mater. Des.*, 140(2018), p. 286.

[17] M. Amir, U. Kurtan, and A. Baykal, Synthesis and application of magnetically recyclable nanocatalyst Fe_3O_4@Nico@Cu in the reduction of azo dyes, *Chin. J. Catal.*, 36(2015), No. 8, p. 1280.

[18] Y. Liu, X. Chen, J. Li, and C. Burda, Photocatalytic degradation of azo dyes by nitrogen-doped TiO_2 nanocatalysts, *Chemosphere*, 61(2005), No. 1, p. 11.

[19] C.C. Amorim, M.M.D. Leão, R.F.P.M. Moreira, J.D. Fabris, and A.B. Henriques, Performance of blast furnace waste for azo dye degradation through photo-Fenton-like processes, *Chem. Eng. J.*, 224(2013), No. 1, p. 59.

[20] S.D. Kalme, G.K. Parshetti, S.U. Jadhav, and S.P. Govindwar, Biodegradation of benzidine based dye Direct Blue-6 by *Pseudomonas desmolyticum* NCIM 2112, *Bioresour. Technol.*, 98(2007), No. 7, p. 1405.

[21] N. Ertugay and F.N. Acar, Removal of COD and color from Direct Blue 71 azo dye wastewater by Fenton's oxidation: Kinetic study, *Arabian J. Chem.*, 10(2017), Suppl. 1, p. S1158.

[22] I.K. Konstantinou and T.A. Albanis, TiO_2-assisted photocatalytic degradation of azo dyes in aqueous solution: kinetic and mechanistic investigations: A review, *Appl. Catal. B*, 49(2004), No. 1, p. 3.

[23] Y. Tang, Y. Shao, N. Chen, X. Liu, S.Q. Chen, and K.F. Yao, Insight into the high reactivity of commercial Fe–Si–B amorphous zero-valent iron in degrading azo dye solutions, *RSC Adv.*, 5(2015), No. 43, p. 34032.

[24] R.V. Solomon, I.S. Lydia, J.P. Merlin, and P. Venuvanalingam, Enhanced photocatalytic degradation of azo dyes using nano Fe_3O_4, *J. Iran. Chem. Soc.*, 9(2012), No. 2, p. 101.

[25] W. Li, S.K. Guan, J. Chen, J.H. Hu, S. Chen, L.G. Wang, and S.J. Zhu, Preparation and in vitro degradation of the composite coating with high adhesion strength on biodegradable Mg–Zn–Ca alloy, *Mater. Charact.*, 62(2011), No. 12, p. 1158.

[26] J.Q. Wang, Y.H. Liu, M.W. Chen, D.V. Louzguine-Luzgin, A. Inoue, and J.H. Perepezko, Excellent capability in degrading azo dyes by MgZn-based metallic glass powders, *Sci. Rep*., 2(2012), No. 5, art. No. 418.

[27] X.D. Qin, Z.W. Zhu, G. Liu, H.M. Fu, H.W. Zhang, A.M. Wang, H. Li, and H.F. Zhang, Ultrafast degradation of azo dyes catalyzed by cobalt-based metallic glass, *Sci. Rep.*, 5(2015), No. 2, art. No. 18226.

[28] Y.F. Zhao, J.J. Si, J.G. Song, Q. Yang, and X.D. Hui, Synthesis of Mg–Zn–Ca metallic glasses by gas-atomization and their excellent capability in degrading azo dyes, *Mater. Sci. Eng. B*, 181(2014), No. 181, p. 46.

[29] H.Y. Shu, M.C. Chang, C.C. Chen, and P.E. Chen, Using resin supported nano zero-valent iron particles for decoloration of Acid Blue 113 azo dye solution, *J. Hazard. Mater.*, 184(2010), No. 1-3, p. 499.

[30] Y. Keum and Q.X. Li, Reduction of nitroaromatic pesticides with zero-valent iron, *Chemosphere*, 54(2004), No. 3, p. 255.

[31] C.F. Lee and T.T. Shun, Effect of Fe content on microstructure and mechanical properties of $Al_{0.5}$ $CoCrFe_xNiTi_{0.5}$ high-entropy alloys, *Mater. Charact.*, 114(2016), No. 2, p. 179.

[32] L.X. Yin, D.D. Zhang, J. Wang, J.F. Huang, X.G. Kong, J.M. Fang, and F. Zhang, Improving sunlight-driven photocatalytic activity of ZnO nanostructures upon decoration with Fe(III) cocatalyst, *Mater. Charact.*, 127(2017), No. 3, p. 179.

[33] R.R. Eleti, V. Raju, M. Veerasham, S.R. Reddy, and P.P. Bhattacharjee, Influence of strain on the formation of cold-rolling and grain growth textures of an equiatomic HfZrTiTaNb refractory high entropy alloy, *Mater. Charact.*, 136(2018), No. 2, p. 286.

[34] H.T. Zhou, Y.J. Su, N. Liu, F.T. Kong, X.P. Wang, X. Zhang, and Y.Y. Chen, Modification of microstructure and properties of Ti–47Al–2Cr–4Nb–0.3W alloys fabricated by SPS with trace multilayer graphene addition, *Mater Charact.*, 138(2018), No. 1, p. 1.

[35] Z.B. Cai, G. Jin, X.F. Cui, Z. Liu, W. Zheng, Y. Li, and L.Q. Wang, Synthesis and microstructure characterization of Ni–Cr–Co–Ti–V–Al high entropy alloy coating on Ti–6Al–4V substrate by laser surface alloying, *Mater. Charact.*, 120(2016), No. 3, p. 229.

[36] O. Maulik and V. Kumar, Synthesis of $AlFeCuCrMg_x$ (x = 0, 0.5, 1, 1.7) alloy powders by mechanical alloying, *Mater. Charact.*, 110(2015), No. 2, p. 116.

[37] H. Kusic, N. Koprivanac, and L. Srsan, Azo dye degradation using Fenton type processes assisted by UV irradiation: A kinetic study, *J. Photochem. Photobiol. A*, 181(2006), No. 2-3, p. 195.

[38] C.Q. Zhang, Z.W. Zhu, H.F. Zhang, and Z.Q. Hu, Rapid reductive degradation of azo dyes by a unique structure of amorphous alloys, *Chin. Sci. Bull.*, 56(2011), No. 36, p. 3988.

[39] C.Q. Zhang, H.F. Zhang, M.Q. Lv, and Z.Q. Hu, Decolorization of azo dye solution by Fe–Mo–Si–B amorphous alloy, *J. Non-Cryst Solids*, 356(2010), No. 33-34, p. 1703.

[40] J. Wang, Y. Liu, M. Chen, G. Xie, D.V. Louzguine-Luzgin, A. Inoue, and J.H. Perepezko, Rapid degradation of azo dye by Fe-based metallic glass powder, *Adv. Funct. Mater.*, 22(2012), No. 12, p. 2567.

[41] J. Fan, Y. Guo, J. Wang, and M. Fan, Rapid decolorization of azo dye methyl orange in aqueous solution by nanoscale zerovalent iron particles, *J. Hazard. Mater.*, 166(2009), No. 2-3, p. 904.